Second International Symposium on Marine Propulsors
smp'11, Hamburg, Germany, June 2011

Open-Water Thrust and Torque Predictions of a Ducted Propeller System With a Panel Method

J. Baltazar[1], J.A.C. Falcão de Campos[1] and J. Bosschers[2]

[1]Marine Environment and Technology Center (MARETEC),
Department of Mechanical Engineering, Instituto Superior Técnico (IST), Lisbon, Portugal
[2]Maritime Research Institute Netherlands (MARIN), Wageningen, The Netherlands

ABSTRACT

This paper discusses several modelling aspects which are important for the performance predictions of a ducted propulsor with a low-order Panel Method. The aspects discussed are the alignment of the wake geometry, the influence of the duct boundary layer on the wake pitch and the influence of a transpiration velocity through the gap. The analysis is carried out for propeller Ka4-70 operating without and inside a modified duct 19A, in which the rounded trailing edge is replaced by a sharp trailing edge. Experimental data for the thrust and torque are used to validate the numerical results. The pitch of the tip vortex is found to have a strong influence on the propeller and duct loads. A good agreement with the measurements is achieved when the wake alignment is corrected for the presence of the duct boundary layer.

Keywords

Ducted Propeller, Panel Method, Thrust and Torque Predictions

1 INTRODUCTION

The ability to accurately predict the thrust and torque of a ducted propeller in open-water conditions is very important for a calculation method used in the design stage. RANSE methods have been progressively introduced for the calculation of ducted propeller systems, meeting considerable success in predicting open-water characteristics for the well-known Ka-series (Sanchez-Caja et al 2000), (Abdel-Maksoud & Jeinke 2003) and (Krasilnikov et al 2007). However, due to their relative complexity and time requirements, they are not yet routinely used in the design process, which is often still based on the use of inviscid flow methods.

Various numerical methods based on inviscid (potential) flow theory have been proposed for the analysis of ducted propellers. Examples are the combination of a Panel Method, also known as Boundary Element Method, to model the duct with a vortex lattice method for the propeller (Kerwin et al 1987), and a Panel Method for the complete ducted propeller system operating in unsteady flow conditions including blade sheet cavitation (Lee & Kinnas 2006). Both methods applied a transpiration velocity model for the gap flow between propeller blade tip and duct inner surface, and analysed a duct with a sharp trailing edge.

These references show that the application of inviscid flow models to ducted propellers, albeit of great usefulness, may meet some serious limitations related to the occurrence of flow regions where viscous effects cannot be ignored and have to be modelled in some way for the correct prediction of the ducted propeller thrust and torque. One of such region concerns the gap flow, which has a strong influence on the propeller and duct circulation distribution, and therefore, on the distribution of loading between propeller and duct, as studied in detail by Baltazar & Falcão (2009). In addition, there may be a considerable interaction between the vorticity shed from the propeller blade tips and the boundary layer developing on the duct inner side, as found in the works of Krasilnikov et al (2007) and Rijpkema & Vaz (2011). This effect has not been studied before with potential flow methods and its importance is therefore unknown.

The purpose of this paper is to show the importance of an efficient and robust method for the vortex pitch alignment, including the effect of gap modelling and the effect of duct boundary layer. The computational results are compared with open-water data measured at MARIN for the ducted propeller Ka4-70 with $P/D = 1.0$ operating without and inside a modified duct 19A Bosschers & von der Veeken (2008). The section geometry of this duct, denoted as duct 19Am was obtained by replacing the round trailing edge of the duct 19A (van Manen & Oosterveld 1966) by a sharp trailing edge. This sharp trailing edge allows the application of a classical Kutta condition for the prediction of the duct circulation.

Details of the mathematical formulation of the Panel Method are shown in Section 2. The numerical models for the gap region and the interaction with the duct boundary layer are presented in Section 3. This section also discusses the two wake alignment methods that have been investigated, which are a rigid wake model with prescribed geometry and an iterative wake alignment model. The influence of these models on the results and the comparison with the experimental data is shown in Section 4. In Section 5 the

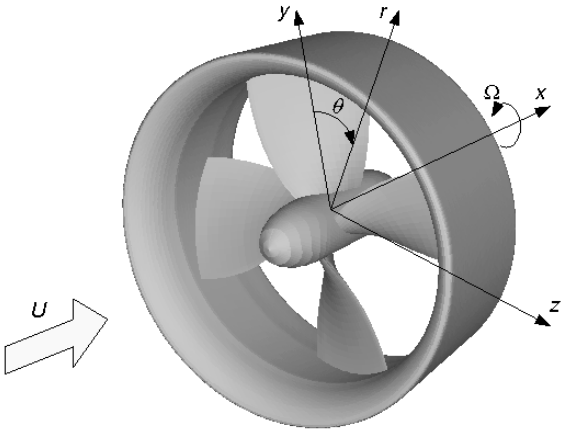

Figure 1: Propeller coordinate system.

main conclusions are drawn.

2 MATHEMATICAL FORMULATION

2.1 Potential Flow Problem

Consider a propeller of radius R rotating with constant angular velocity Ω inside a duct and advancing with constant axial speed U along its axis in an incompressible ideal fluid of constant density ρ at rest in a domain extending to infinity in all directions. The propeller is made of K blades symmetrically distributed around an axisymmetric hub. The duct is also considered to be axisymmetric of inner radius at the propeller plane $R_d \geq R$ which defines a gap height $h = R_d - R$. The flow field is steady in a reference frame rotating with the propeller blades around its axis. Figure 1 shows the coordinate system used to describe the propeller geometry and the fluid domain around the ducted propeller.

We introduce a Cartesian coordinate system (x, y, z) rotating with the propeller blades, with the positive x - axis direction opposite to the propeller axial motion, the y - axis coincident with the propeller reference line, passing through the reference point of the root section of the blade $k = 1$, and the z - axis completing the right-hand system. We use a cylindrical coordinate system (x, r, θ) related to the Cartesian system by the transformation:

$$y = r\cos\theta, \quad z = r\sin\theta. \tag{1}$$

In the coordinate system rotating with the propeller blades, the flow is steady and assuming that the flow is irrotational then, the velocity field $\mathbf{V}(x, y, z)$ may be described by a perturbation potential $\phi(x, y, z)$ in the form:

$$\mathbf{V} = \mathbf{U}_\infty + \nabla\phi, \tag{2}$$

where

$$\mathbf{U}_\infty = U\mathbf{e}_x + \Omega r\mathbf{e}_\theta \tag{3}$$

is the undisturbed onset velocity in the rotating frame.

The perturbation potential satisfies the Laplace equation:

$$\nabla^2\phi = 0. \tag{4}$$

The boundary of domain consists of the blade surfaces $\mathcal{S}_\mathcal{B}$, the duct surface $\mathcal{S}_\mathcal{D}$ and the hub surface $\mathcal{S}_\mathcal{H}$. The kinematic boundary condition,

$$\frac{\partial\phi}{\partial n} \equiv \mathbf{n}\cdot\nabla\phi = -\mathbf{n}\cdot\mathbf{U}_\infty \ \text{ on } \ \mathcal{S}_\mathcal{B}\cup\mathcal{S}_\mathcal{D}\cup\mathcal{S}_\mathcal{H}, \tag{5}$$

is satisfied on the blade, duct and hub surfaces, where $\partial/\partial n$ denotes differentiation along the normal and $\mathbf{n}$ is the unit vector normal to the surface directed outward from the body. At infinity the flow disturbance due to the ducted propeller vanishes:

$$\nabla\phi \to 0, \ \text{ if } \ r\to\infty \ \text{ or } \ x\to-\infty. \tag{6}$$

To allow for the existence of circulation around the propeller blades and the duct, vortex sheets are shed from the trailing edge of the blades and the duct. The boundary conditions on the vortex sheet surfaces $\mathcal{S}_\mathcal{W}$ are the tangency of the fluid velocity on each side of the sheet and the continuity of the pressure across the sheet. In steady flow these conditions are:

$$\frac{\partial\phi_+}{\partial n} = \frac{\partial\phi_-}{\partial n} = -\mathbf{n}\cdot\mathbf{U}_\infty, \ \ p_+ = p_- \ \text{ on } \ \mathcal{S}_\mathcal{W}, \tag{7}$$

where p is the pressure and the indices $+$ and $-$ denote the two sides of the vortex sheets, taken, respectively, on the side of the back (normally the suction side) and face (normally the pressure side) of the blade at the trailing edge, and on the inner side and outer side of the duct at the trailing edge. In the case of the propeller blade, the unit normal to the vortex sheet is defined pointing from the face $(-)$ to the back $(+)$ side of the blade. In the case of the duct, the unit normal to the vortex sheet is defined pointing from the outer $(-)$ to the inner $(+)$ side of the duct.

In order to specify uniquely the circulation around the blades and duct, it is necessary to impose the Kutta condition at the blade trailing edge and at the duct trailing edge. The Kutta condition states that the velocity must remain finite

$$|\nabla\phi| < \infty \tag{8}$$

at a sharp trailing edge.

Applying Green's second identity, assuming for the interior region to $\mathcal{S}_\mathcal{B}\cup\mathcal{S}_\mathcal{D}\cup\mathcal{S}_\mathcal{H}$, $\bar{\phi} = 0$, we obtain the integral representation of the perturbation potential at a point p on the body surface,

$$\begin{aligned} 2\pi\phi(p) = &\iint\limits_{\mathcal{S}_\mathcal{B}\cup\mathcal{S}_\mathcal{D}\cup\mathcal{S}_\mathcal{H}} \left[G\frac{\partial\phi}{\partial n_q} - \phi(q)\frac{\partial G}{\partial n_q}\right] dS \\ &- \iint\limits_{\mathcal{S}_\mathcal{W}} \Delta\phi(q)\frac{\partial G}{\partial n_q} dS, \ \ p\in\mathcal{S}_\mathcal{B}\cup\mathcal{S}_\mathcal{D}\cup\mathcal{S}_\mathcal{H} \end{aligned} \tag{9}$$

where $G(p,q) = -1/R(p,q)$, $R(p,q)$ is the distance between the field point p and the point q on the boundary $\mathcal{S}_\mathcal{B}\cup\mathcal{S}_\mathcal{D}\cup\mathcal{S}_\mathcal{H}\cup\mathcal{S}_\mathcal{W}$. With the $\partial\phi/\partial n_q$ on the surfaces $\mathcal{S}_\mathcal{B}$, $\mathcal{S}_\mathcal{D}$ and $\mathcal{S}_\mathcal{H}$ known from the Neumann boundary condition on the body surface, Equation (5), the Equation (9) is a Fredholm integral equation of the second kind in the

dipole distribution $\mu(q) = -\phi(q)$ on the surfaces $\mathcal{S}_\mathcal{B}$, $\mathcal{S}_\mathcal{D}$ and $\mathcal{S}_\mathcal{H}$. The Kutta condition, Equation (8), yields the additional relationship between the dipole strength $\Delta\phi(q)$ in the wake surfaces $\mathcal{S}_\mathcal{W}$ and the surface dipole strength at the blade and duct trailing edges.

2.2 Velocity, Pressure and Forces

The velocity on the surface is obtained by differentiation of the surface potential distribution. From Bernoulli's equation, the pressure coefficient C_p can be determined from:

$$C_p = \frac{p - p_\infty}{1/2\rho U_\infty^2} = 1 - \left(\frac{|\mathbf{V}|}{U_\infty}\right)^2, \tag{10}$$

where p_∞ is the pressure of the undisturbed inflow and $|\mathbf{V}|$ is the total velocity.

The inviscid thrust and torque on the ducted propeller are obtained by integration of the pressure distribution on the blade and duct surfaces. The propeller operation conditions are defined by a single non-dimensional parameter: the advance coefficient $J = U/nD$, where $n = \Omega/2\pi$ is the rate of revolution and $D = 2R$ the propeller diameter. The non-dimensional thrust and torque of the ducted propeller system are given by the propeller thrust coefficient K_{T_P}, the duct thrust coefficient K_{T_D} and the torque coefficient K_Q:

$$K_{T_P} = \frac{T_P}{\rho n^2 D^4}, K_{T_D} = \frac{T_D}{\rho n^2 D^4}, K_Q = \frac{Q}{\rho n^2 D^5}, \tag{11}$$

where T_P is the propeller thrust, T_D the duct thrust and Q the propeller torque. The ducted propeller efficiency is given by:

$$\eta = \frac{U\left(T_P + T_D\right)}{2\pi n Q}. \tag{12}$$

3 NUMERICAL METHOD

3.1 Surface Discretisation

For the numerical solution of the integral equation, Equation (9), we discretise the blade surfaces $\mathcal{S}_\mathcal{B}$, the duct surface $\mathcal{S}_\mathcal{D}$, the hub surface $\mathcal{S}_\mathcal{H}$ and the wake surfaces $\mathcal{S}_\mathcal{W}$ in bi-linear quadrilateral panels. The blade is discretised in the spanwise radial direction by a number of strips, extending chordwise from the blade leading edge to the trailing edge. Cosine spacing in the radial and chordwise directions is used. The duct surface is divided into three regions: between, upstream and downstream of the blades. The regions between and downstream of the blades are discretised along the axial direction with the same panel spacing of the blade tip section and blade wake tip section, respectively. The region upstream of the blades is discretised along the axial direction with a Vinokur stretching function, (Vinokur 1983). Equidistant angular spacing is used in circumferential direction. For the discretisation of the hub surface, an elliptical grid generator is used (Sorensen 1986). The blade and duct wake surfaces are discretised in the spanwise and circumferential directions, extending downstream from the trailing edge the corresponding strips on the propeller blade and duct surfaces.

3.2 Solution of the Integral Equation

The integral equation, Equation (9), is solved by the collocation method with the element centre point as collocation point. We assume a constant strength of the dipole and source distributions on each element. The influence coefficients are determined analytically using the formulations of Morino and Kuo (1974).

3.3 Wake Models

Two wake models are considered: a rigid wake model and a wake alignment model for the blade wake where the pitch of the vortex lines are aligned with the local fluid velocity.

In the rigid wake model, the geometry of the wake surfaces are specified empirically. For the blade wake, the pitch of the vortex lines is assumed constant along the axial direction and equal to the blade pitch. However, contraction of the blade wake is prescribed by an empirical formulation, following Hoshino (1989). The radial variation of the helicoidal lines is occurring in a transition wake region, with a length of $2R$, and is kept constant further downstream. For the duct, the wake leaves the trailing edge at the bisector. The value of the dipole strength at the blade and duct trailing edges is determined by the application of an iterative pressure Kutta condition, requiring that the pressure is equal on both sides of the blade and duct panels adjacent to the trailing edge.

In the wake alignment model, the corner points of the blade wake grid panels are displaced with the mean fluid velocity. At the $(n+1)^{\text{th}}$ iteration, the geometry in cylindrical coordinates of the wake strip $i+1$ can be determined by using an Euler scheme:

$$\begin{cases} x_{i+1}^{(n+1)} = x_i^{(n)} + V_x\left(x_i^{(n)}, r_i^{(n)}, \theta_i^{(n)}\right)\Delta t \\ r_{i+1}^{(n+1)} = r_i^{(n)} + V_r\left(x_i^{(n)}, r_i^{(n)}, \theta_i^{(n)}\right)\Delta t \\ \theta_{i+1}^{(n+1)} = \theta_i^{(n)} + V_\theta\left(x_i^{(n)}, r_i^{(n)}, \theta_i^{(n)}\right)\Big/ r_i^{(n)}\Delta t \end{cases}. \tag{13}$$

where V_x, V_r and V_θ are the components of the mean vortex sheet velocity along the axial, radial and circumferential directions, respectively, and Δt is the time step for the Euler vortex convection scheme. The first wake strip ($i = 1$) corresponds to the blade trailing edge. To control the wake alignment stability, the radial coordinates of the blade wake grid are kept constant during the iterative process. Hence,

$$r_{i+1}^{(n+1)} = r_i^{(n)} + \Delta r_i^{(n)}, \tag{14}$$

where

$$\Delta r_i^{(n)} = r_{i+1}^{(0)} - r_i^{(0)}. \tag{15}$$

The new axial and circumferential coordinates $x_{i+1}^{(n+1)}$ and $\theta_{i+1}^{(n+1)}$ are calculated using an Euler scheme:

$$\begin{cases} \tilde{x}_{i+1}^{(n+1)} = x_i^{(n)} + V_x\left(x_i^{(n)}, r_i^{(n)}, \theta_i^{(n)}\right)\Delta t \\ \tilde{\theta}_{i+1}^{(n+1)} = \theta_i^{(n)} + V_\theta\left(x_i^{(n)}, r_i^{(n)}, \theta_i^{(n)}\right)\Big/ r_i^{(n)}\Delta t \end{cases}. \tag{16}$$

The non-dimensional time step $\Delta\theta = \Omega\Delta t$ is introduced, which can also be expressed in terms of the number of time steps per propeller revolution $N_\theta = \frac{2\pi}{\Delta\theta}$. Note that in the wake alignment model the downstream part of the duct is remeshed at each iteration of the propeller and duct vortex wakes alignment.

3.4 Gap Flow Models

Two different models for the potential flow in the gap region are considered: a closed gap with zero gap width and a gap flow model with transpiration velocity.

In the closed gap model, the blade and duct grids match in the tip region. In this case, the flow is not allowed to pass between the blade tip and the duct inner surface. The blade wake connects to the duct inner surface down to the duct trailing edge.

In the gap model with transpiration velocity, a partial flow between the blade tip and the duct inner surface is allowed to pass in the gap region. The procedure proposed by Hughes (1997) is implemented in the current method, where the gap flow is treated as a two-dimensional orifice. The velocity in the gap region can be related to the difference in pressure across the blade tip using Bernoulli's equation. The reduction in the flow from losses in the orifice is expressed in terms of an empirical discharge coefficient from the total volume flow rate through the gap Q_G and the pressure difference across the gap Δp as:

$$C_Q = \frac{Q_G}{h}\sqrt{\frac{\rho}{2\Delta p}}. \tag{17}$$

From Equation (17), the mean velocity through the gap at a given chordwise location can be expressed in terms of the difference in pressure between the pressure and suction sides of the blade at that location:

$$\omega_R = C_Q\sqrt{\frac{2\Delta p}{\rho}} = |\mathbf{U}_\infty| C_Q\sqrt{\Delta C_p}. \tag{18}$$

where ω_R is the mean relative flow velocity through the gap and ΔC_p is the pressure difference at the blade tip in terms of the pressure coefficient defined by Equation (10).

To incorporate this expression for the mean velocity into the Panel Method, an additional strip of panels along the blade tip is introduced which closes the gap. This wake strip continues past the duct trailing edge, connecting the duct wake with the blade wake. The dipole strength on the last wake strip is also determined from the Kutta condition. In the case of a closed gap, the boundary condition on the gap panels sets the source strength to cancel the normal component of the inflow velocity, (Equation 5). To allow for the existence of a transpiration velocity through the gap, the boundary condition on the gap strip becomes:

$$\frac{\partial\phi}{\partial n} = -\mathbf{U}_\infty\cdot\mathbf{n} + |\mathbf{U}_\infty| C_Q\sqrt{\Delta C_p}\mathbf{n}\cdot\mathbf{n}_c, \tag{19}$$

where $\mathbf{n}_c$ is the unit normal vector to the mean camber line at the gap strip on the same chordwise position of the panel.

The value of ΔC_p is obtained by an iterative procedure. First, the potential flow problem is solved as if the gap were completely closed, and Equation (5) is used to impose the kinematic boundary condition on the gap strip. The pressure distribution is then computed by differentiating the potential using a finite difference scheme. The potential flow problem is solved again with the kinematic boundary condition on the gap strip specified by Equation (19). The pressures on the gap strip are then recomputed and used to update the boundary condition on the gap panels. The solution process will be repeated until a specified convergence criterion is met.

3.5 A Simple Model for the Interaction of the Blade Wake With the Duct Boundary Layer

A simple model for the interaction between the blade wake and the boundary layer on the duct inner side is implemented as well. Due to the duct boundary layer, a reduction in the axial velocity may be taken into account in the convection of blade vorticity in the wake alignment model. Considering δ as the duct boundary layer thickness and assuming a power law distribution for the velocity profile, we have:

$$\frac{V_x\left(R_d - r\right)}{V_x\left(\delta\right)} = \left(\frac{R_d - r}{\delta}\right)^{\frac{1}{n}}. \tag{20}$$

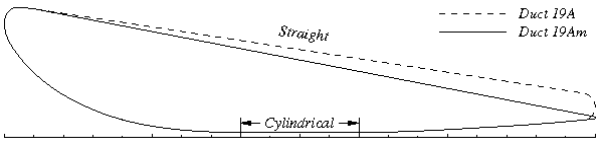

Figure 2: Profiles of duct 19A and 19Am.

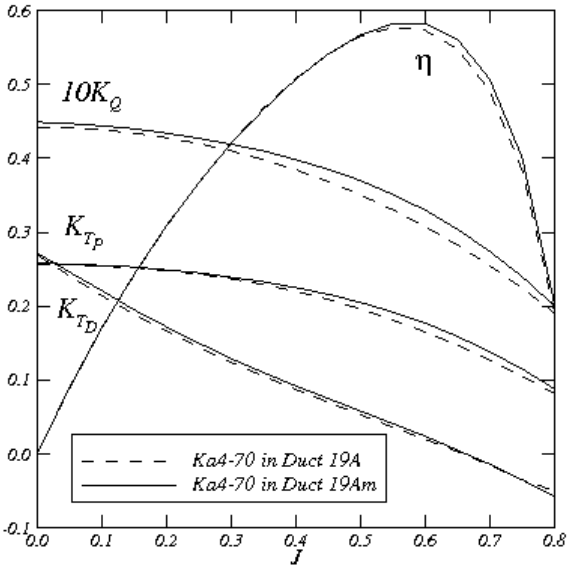

Figure 3: Experimental open-water characteristics of propeller Ka4-70 in duct 19A and duct 19Am.

To correct the potential flow velocities in the blade wake, a linear variation of the axial velocity is considered in the gap region, $R \leq r \leq R_d$. The corrected axial velocity

at the duct surface, $V_x(0)$ is calculated by extrapolation from its value at the gap, $V_x(h)$, and at the edge of the duct boundary layer, $V_x(\delta)$. The velocity at the edge of the duct boundary layer is identical to the velocity on the duct surface in the potential flow method. A correction factor for the velocity at the duct surface can be derived from Equation (20) and is given by:

$$\frac{V_x(0)}{V_x(\delta)} = \left(\frac{h}{\delta}\right)^{\frac{1}{n}} - \frac{1-\left(\frac{h}{\delta}\right)^{\frac{1}{n}}}{1-\frac{h}{\delta}}\frac{h}{\delta}. \qquad (21)$$

4 RESULTS

4.1 General

Results are presented for the propeller Ka4-70 without and inside the duct 19Am. The propeller Ka4-70 is a four-bladed propeller of the Kaplan type with a large chord at the blade tip. A pitch-diameter ratio of $P/D = 1.0$ is considered. The duct 19Am is based on duct 19A, modified such that the trailing edge is almost sharp. The particulars of the Ka-series and the duct 19A section geometry can be found in Kuiper (1992). The section geometry of the duct 19Am is given in Bosschers and van der Veeken (2008), which also contains the results of the experiments performed at MARIN in the Netherlands. The gap between the duct inner surface and the blade tip is uniform and equal to 0.83% of the propeller radius. The profiles of the duct 19A and 19Am are compared in Figure 2. The comparison of the experimental open-water characteristics of the ducted propeller system with duct 19A (Kuiper 1992) and with duct 19Am (Bosschers and van der Veeken 2008) is presented in Figure 3.

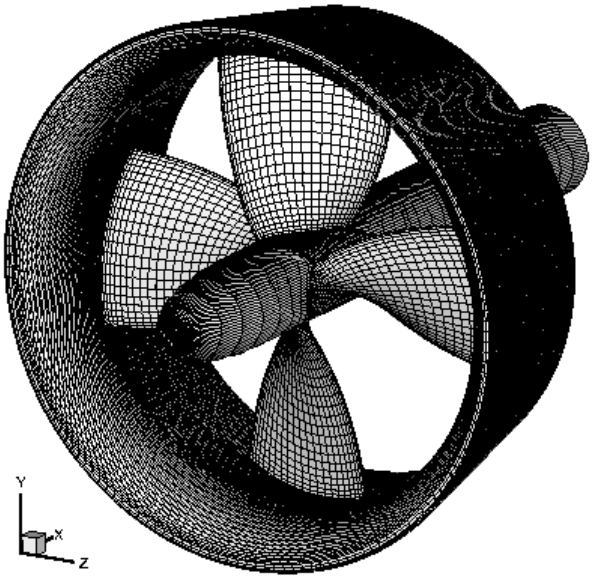

Figure 4: Panel arrangement for propeller Ka4-70 inside duct 19Am. 50×25 panels on each blade; 142×160 panels on the duct; 55×80 panels on the hub.

Figure 4 shows a typical panel arrangement of propeller Ka4-70 inside the duct 19Am with an open-water hub. Calculations were carried out with the rigid wake model and wake alignment model. The wake geometries were obtained after 5 iterations of the wake alignment model using $N_\theta = 90$ time steps per revolution, which leads to an angular step of 4 degrees. For the ducted propeller case, a transpiration velocity gap model with a discharge coefficient equal to $C_Q = 0.84$ (Hughes 1997) and a closed gap model were considered. A specified tolerance of $|\delta(\Delta C_p)_{GAP}| < 10^{-2}$ on the gap strip control points was applied as convergence criterion, corresponding to approximately 20 iterations for the transpiration velocity. In general, the iterative pressure Kutta condition converged after 5 iterations to a precision of $|\Delta C_p| \leq 10^{-3}$. In the iterative procedure to deal with non-linearities of the numerical method, the outer loop is the wake alignment model, the middle loop is the transpiration velocity gap model and the inner loop is the iterative pressure Kutta condition.

4.2 Ka4-70 Without Duct

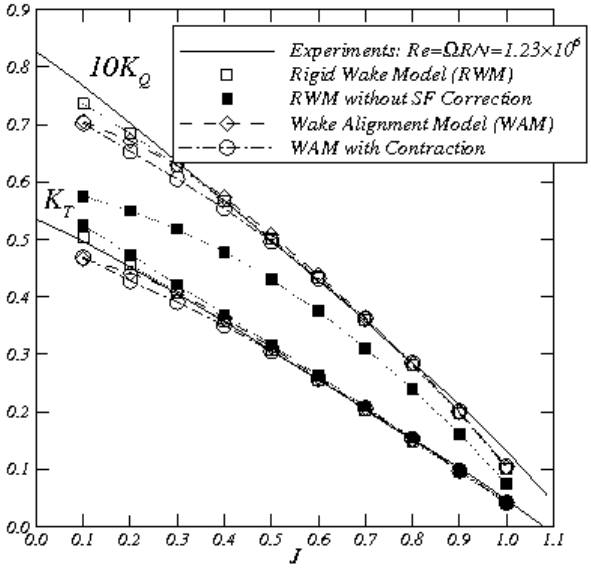

Figure 5: Thrust and torque coefficients for propeller Ka4-70 showing the influence of the wake alignment model and the leading edge suction force (SF) correction.

First, the numerical results are presented for the Ka4-70 propeller without duct in uniform flow using the rigid wake model and the wake alignment model without and with empirical contraction. Figure 5 shows the comparison of the thrust and torque coefficients with experimental data from the open-water tests. A section viscous drag coefficient of 0.007 and a simple model for suppression of the leading edge suction force between sections $r/R = 0.7$ and $r/R = 1.0$ were used for all computations. By applying a leading edge suction force correction, a significant increase of the torque coefficient at low advance ratio and a decrease in the thrust coefficient are obtained. Small differences between the wake models are seen with the exception of the low advance ratios. In this case, a reduction of the force coefficients is observed with wake alignment models for low advance ratios. These differences are related to the difficulty in obtaining converged and smooth aligned wake surfaces when large induced velocities are present. In general,

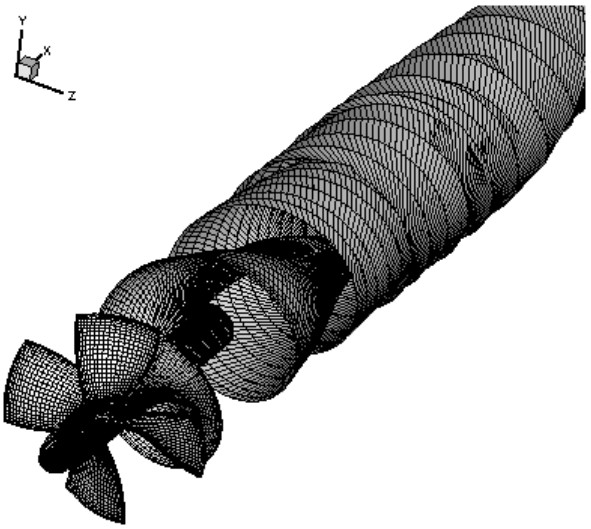

Figure 6: Panel arrangement for propeller Ka4-70 at $J = 0.5$ for the wake alignment model with empirical contraction. Note that the only one blade wake grid (400×25) is shown.

a fair to good agreement is seen between the numerical predictions and the experimental data. The reasons for the underprediction of the force coefficients at low advance ratios are probably the limitations of the wake alignment model and the flow separation from the propeller blades which is modelled by a simple suppression of the suction force.

Figure 6 presents the panel arrangement including the aligned wake for the advance ratio $J = 0.5$. To control the convergence and smoothness of the wake grid, the tip vortex roll-up phenomenon is not modelled with the present alignment method. Figure 7 shows the blade circulation and pressure distribution at the radial section $r/R = 0.99$. Similar circulation and pressure distributions are obtained between all wake models. Please note that large suction peaks near the blade leading edge are obtained in the inviscid flow solution, which are physically not realistic.

4.3 Ka4-70 Inside Duct 19Am

Secondly, the effect of the gap and the wake alignment models are investigated for propeller Ka4-70 inside duct 19Am. Calculations are presented for the rigid wake model and for the wake alignment model without and with correction of the axial velocity due to the duct boundary layer. The thickness of the duct boundary layer δ/R is assumed to be 4%, corresponding to $h/\delta = 0.21$. A power law velocity profile with $n = 7$ is assumed.

Figure 8 shows the comparison of the predicted thrust and torque coefficients with experimental data from the open-water tests. A section viscous drag coefficient of 0.007 was used for all computations for the propeller. No viscous drag correction to the duct thrust has been applied. The differences between the closed and transpiration gap models are small. As expected, the closed gap model decreases the propeller/duct load ratio in comparison with the transpiration velocity gap model. The comparison with the experiments shows that the numerical results obtained with the rigid wake model and wake alignment model without

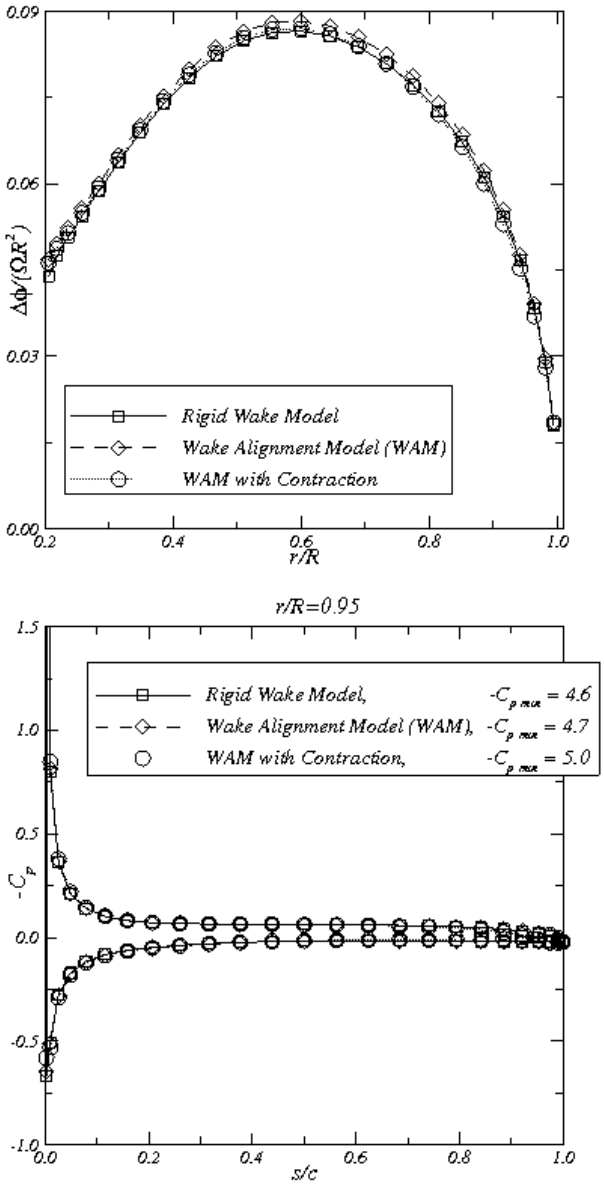

Figure 7: Radial circulation (top) and chordwise pressure (bottom) distributions. Propeller Ka4-70 at $J = 0.5$. Influence of the wake model.

duct boundary layer correction over-predict the propeller thrust and torque coefficients. By applying the axial velocity correction at the tip in the wake alignment model a significative reduction of the propeller thrust and torque coefficients is observed. A good agreement with the measurements may be achieved. The duct thrust coefficient agrees well with the measurements for low advance coefficients. The correction for the duct boundary layer results in an increase of the duct thrust. However, for high advance ratios all models over-predict the duct thrust, which is probably due to the occurrence of flow separation on the outer side of the duct and it is not modelled in the present method. The differences between the measured and the predicted ducted propeller efficiencies are around 6% for the advance ratios lower than $J = 0.6$.

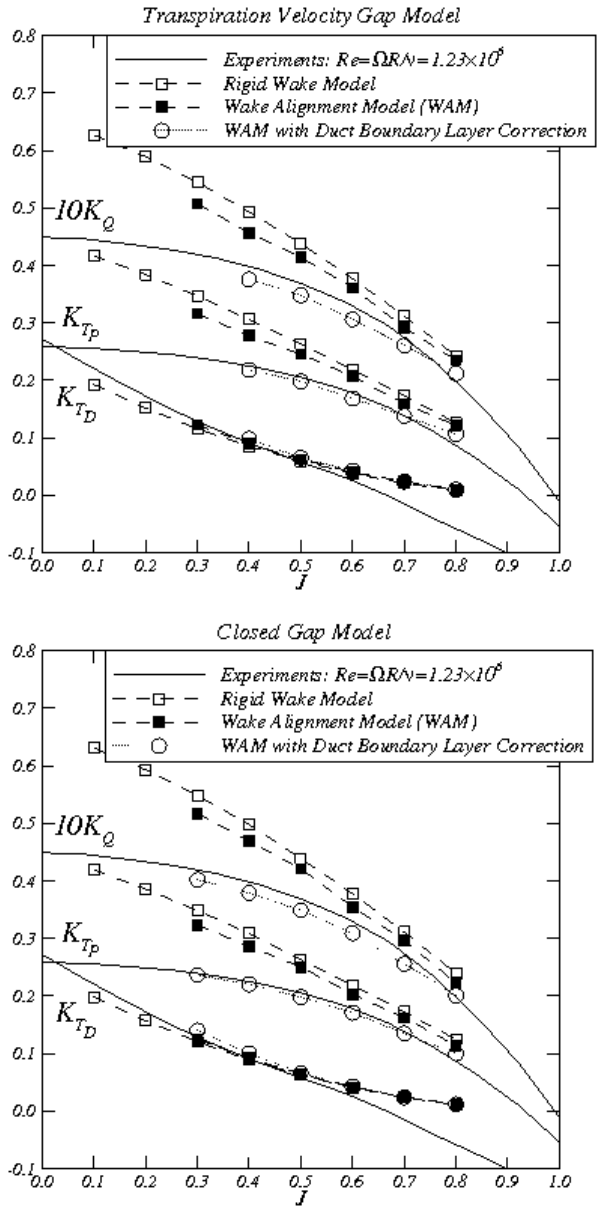

Figure 8: Comparison between predicted thrust and torque coefficients for the Ka4-70 propeller inside duct 19Am. Predictions are presented for the transpiration velocity gap model (top) and the closed gap model (bottom).

Figure 9 presents the panel arrangement including the aligned wake with the duct boundary layer correction. A strong reduction of the blade wake pitch is seen at the tip. The pitch angle of the blade wake at the axial positions $x/R = 0.5$ and $x/R = 2.0$ is illustrated in Figure 10. The correction in the axial velocity due to the duct boundary layer introduces a large reduction of the vortex pitch at the blade wake tip, which is responsible for the significant decrease of propeller thrust and torque and increase of duct thrust.

Figure 11 presents the circulation distributions on the propeller blade and duct. The pressure distributions are shown in Figures 12 and 13 for the gap model with transpiration velocity and closed gap model, respectively. In the closed

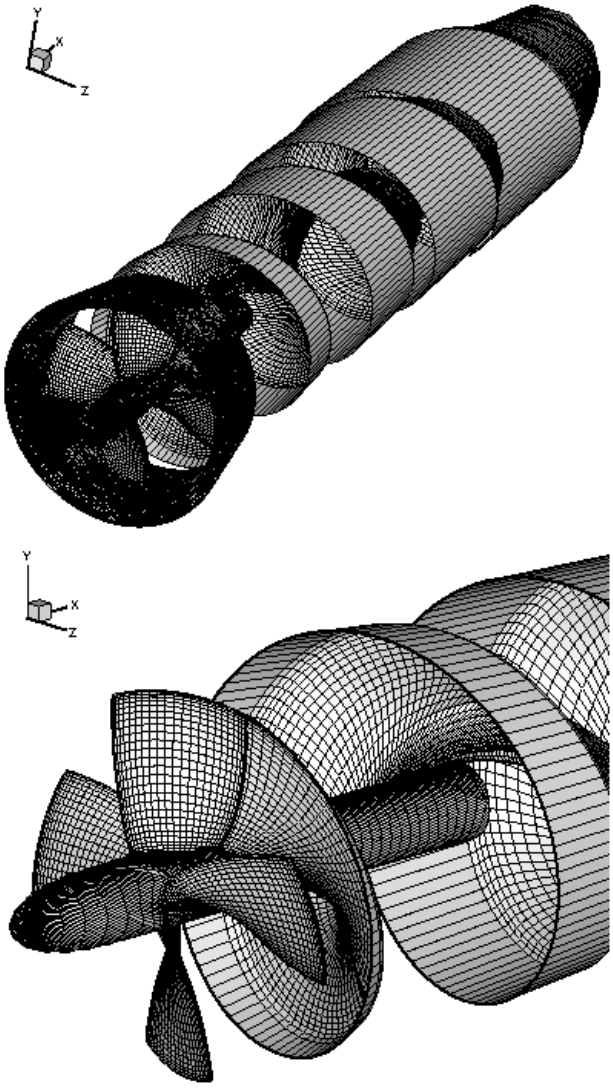

Figure 9: Panel arrangement for propeller Ka4-70 inside duct 19Am at $J = 0.5$. Gap model with transpiration velocity. Wake alignment model with duct boundary layer correction. The duct grid is not shown in the bottom figure.

gap model, the blade circulation at the tip is equal to the duct circulation discontinuity. Note that a finite circulation at the blade tip is also obtained in the gap model with transpiration velocity. Similar results are obtained with the two gap models. Small differences are seen in the blade tip and duct circulations. In the closed gap model the flow is not allowed to pass through the gap and increases the blade tip and duct circulations. For the pressure distributions and propeller forces, similar results are obtained between the two gap models. From the comparison between the wake models, a decrease in the blade circulation is obtained with the wake alignment model, which has the opposite effect on the duct circulation. Although the correction due to the duct boundary layer affects only the blade wake geometry near the tip, a very strong influence on the propeller and duct circulation distributions is obtained. For the blade pressure distribution, no suction peak is seen in the wake alignment model with duct boundary layer correction, indicating a different incidence angle to the blade section. The

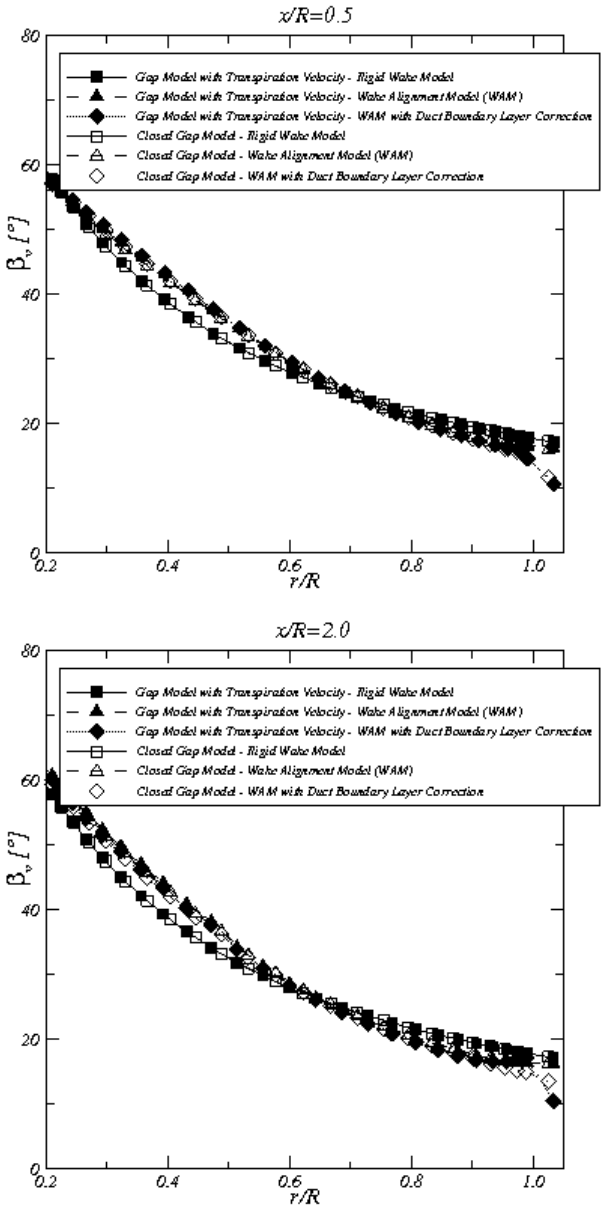

Figure 10: Vortex pitch distributions at $x/R = 0.5$ and $x/R = 2.0$. Influence of gap and wake models. Ka4-70 inside duct 19Am at $J = 0.5$.

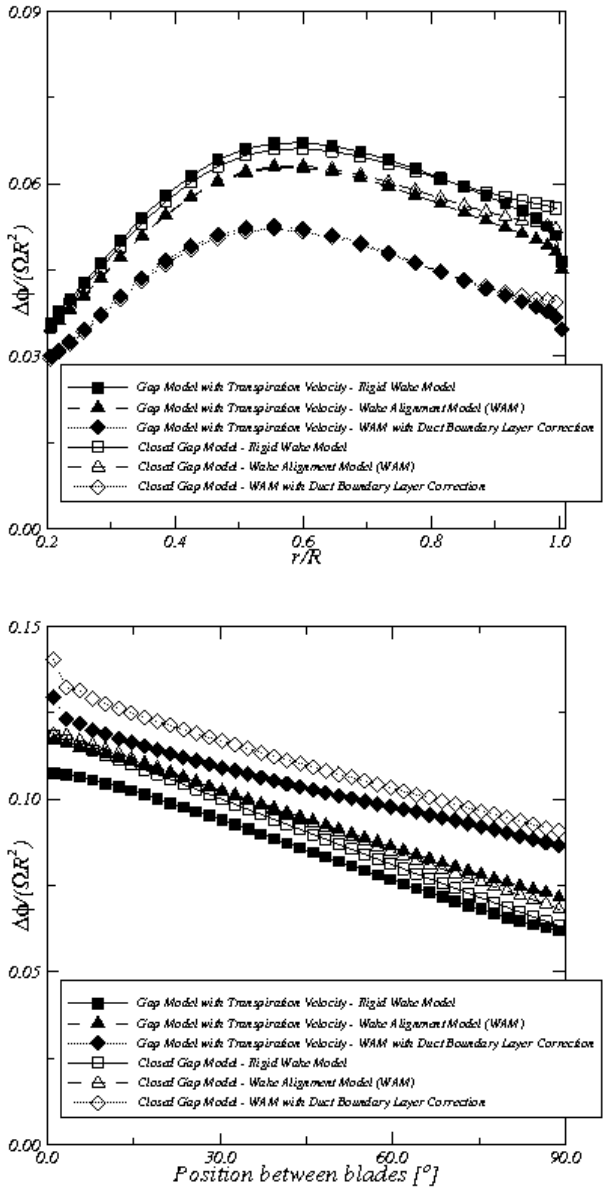

Figure 11: Blade (top) and duct (bottom) circulation distributions. Influence of gap and wake models. Ka4-70 inside duct 19Am at $J = 0.5$.

differences in the duct pressure distributions on the duct inner side in front of the propeller explain the differences in duct thrust.

A sensitivity study for the influence of the duct boundary layer thickness on the predicted thrust and torque coefficients has been performed using the transpiration gap model. The relative differences between the numerical results and the experimental open-water thrust and torque values are presented in Table 1 for various values of the duct boundary layer thickness. It is observed that the influence is very significant and that an increase in boundary layer thickness always leads to a reduction of propeller thrust and torque.

Table 1: Variation with the duct boundary layer thickness of the relative differences between the predicted and experimental (exp) thrust and torque coefficients. Ka4-70 inside duct 19Am at $J = 0.5$. Transpiration velocity gap model.

δ/R	$\frac{K_{T_P}-K_{T_P\exp}}{K_{T_P\exp}}$	$\frac{K_{T_{P+D}}-K_{T_{P+D}\exp}}{K_{T_{P+D}\exp}}$	$\frac{K_Q-K_{Q\exp}}{K_{Q\exp}}$
0.0%	19.8%	17.2%	11.9%
1.0%	8.4%	9.0%	3.2%
2.0%	0.4%	4.0%	-3.0%
3.0%	-1.5%	2.2%	-4.3%
4.0%	-3.3%	0.2%	-5.9%
5.0%	-6.1%	-0.8%	-8.1%

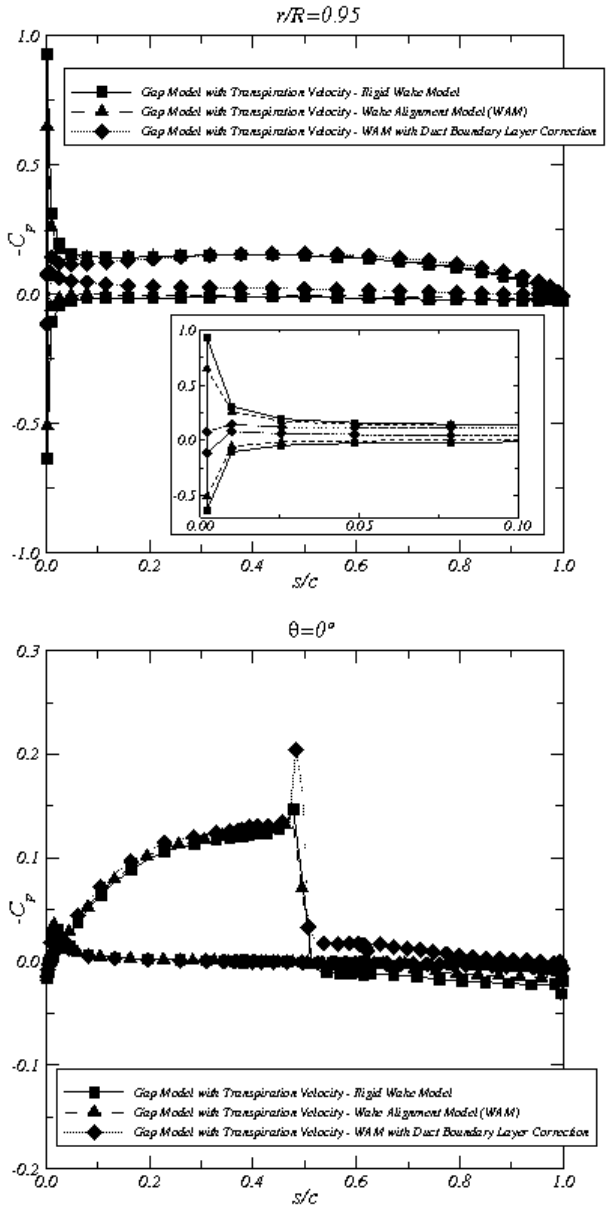

Figure 12: Blade pressure distribution at $r/R = 0.95$ (top). Duct pressure distribution at $\theta = 0$ degrees (bottom). Influence of wake model. Ka4-70 inside duct 19Am at $J = 0.5$. Gap model with transpiration velocity.

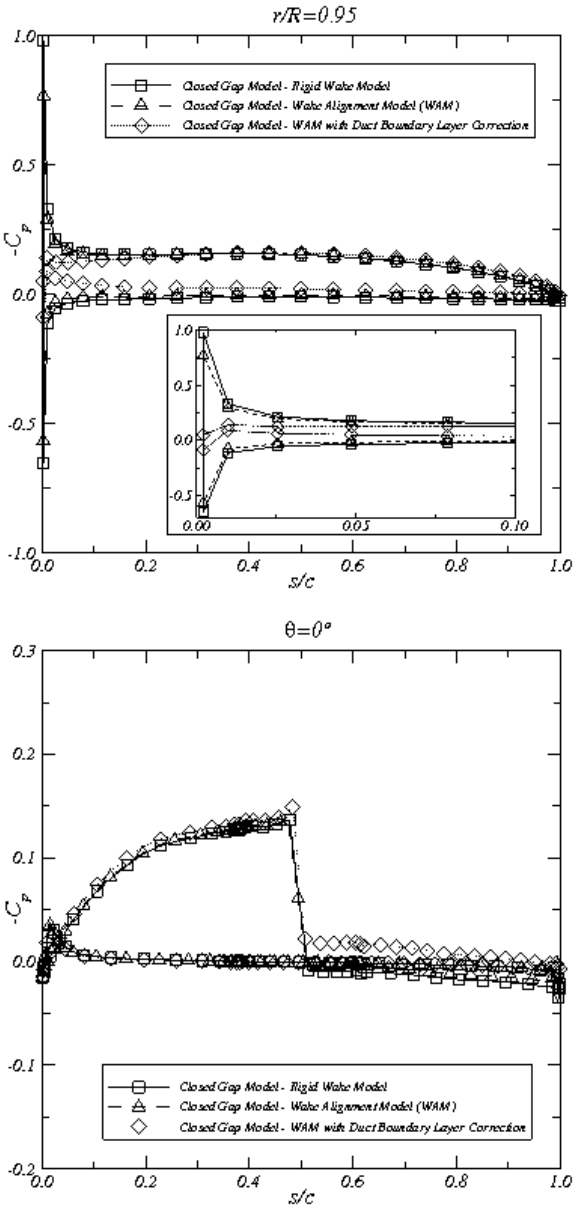

Figure 13: Blade pressure distribution at $r/R = 0.95$ (top). Duct pressure distribution at $\theta = 0$ degrees (bottom). Influence of wake model. Ka4-70 inside duct 19Am at $J = 0.5$. Closed gap model.

5 CONCLUSION

A low-order Panel Method has been used to predict the thrust and torque of propeller Ka4-70 without and inside a modified duct 19A in open water conditions. Calculations were carried out with a rigid wake model and an iterative wake alignment model for the blade wake pitch. For the open propeller, a fair to good agreement is seen between the numerical predictions and the experiments for all wake models. For the ducted propeller, the loading predictions of the duct propeller system were found to be critically dependent on the blade wake pitch, especially at the tip. A model to incorporate the influence of the duct boundary layer on the pitch of tip vorticity was found necessary to correctly predict the open water characteristics of the ducted propeller. This mechanism was not studied before using panel methods but seems plausible from the physical point of view. The quantitative aspects of this mechanism will be investigated in more detail by comparing the results of the present panel method with RANS simulations.

REFERENCES

Abdel-Maksoud, M. & Heinke, H.-J. (2003). 'Scale effects on ducted propellers'. Proceedings of the Twenty-Fourth Symposium on Naval Hydrodynamics, Fukuoka, Japan.

Baltazar, J. & Falcão de Campos, J. A. C. (2009). 'On the modelling of the flow in ducted propellers with a panel method'.

Proceedings of the First International Symposium on Marine Propulsors, Trondheim, Norway.

Bosschers, J. & van der Veeken, R. (2008). Open Water Tests for Propeller Ka4-70 and Duct 19A With a Sharp Trailing Edge, MARIN Report No. 224457-2-VT.

Hoshino, T. (1989). 'Hydrodynamic Analysis of Propellers in Steady Flow Using a Surface Panel Method. 2^{nd} Report: Flow Field Around Propeller'. Journal of The Society of Naval Architects of Japan, **166**,pp.79–91.

Hughes, M. J. (1997). 'Implementation of a special procedure for modeling the tip clearance flow in a panel method for ducted propellers'. Proceedings of the Propellers/Shafting '97 Symposium.

Kerwin, J. E., Kinnas, S. A., Lee, J.-T. & Shih, W.-Z. (1987). 'A surface panel method for the hydrodynamic analysis of ducted propellers'. Transactions of Society of Naval Architects and Marine Engineers **95**.

Krasilnikov, V. I., Sun, J. Y., Zhang, Z. & Hong, F. (2007). 'Mesh Generation Technique for the Analysis of Ducted Propellers Using a Commercial RANSE Solver and its Application to Scale Effect Study'. Proceedings of the 10th Numerical Towing Tank Symposium (NuTTS'07).

Kuiper, G. (1992). 'The Wageningen Propeller Series'. MARIN Publication 92-001.

Lee, H. & Kinnas, S. A. (2006). 'Prediction of cavitating performance of ducted propellers'. Proceedings of the Sixth International Symposium on Cavitation.

Morino, L. & Kuo, C.-C. (1974). "Subsonic Potential Aerodynamics for Complex Configurations: A General Theory'. AIAA Journal **12**(2),pp.191–197.

Rijpkema, D. & Vaz, G. (2011). 'Viscous Flow Computations on Propulsors: Verification, Validation and Scale Effects'. Proceedings of the Developments in Marine CFD.

Sanchez-Caja, A., Rautaheimo, P. & Siikonen, T. (2000). 'Simulation of incompressible viscous flow around a ducted propeller using a RANS equation solver'. Proceedings of the Twenty-Third Symposium on Naval Hydrodynamics.

Sorensen, R. L. (1986). 'Three-Dimensional Elliptic Grid Generation About Fighter Aircraft for Zonal Finite-Difference Computations'. Proceedings of the AIAA 24th Aerospace Sciences Conference.

van Manen, J. D. & Oosterveld, M. W. C. (1966). 'Analysis of Ducted-Propeller Design'. Transactions of Society of Naval Architects and Marine Engineers 74:522–562.

Vinokur, M. (1983). 'On One-Dimensional Stretching Functions for Finite-Difference Calculations'. Journal of Computational Physics **50**,pp.215–234.